

# Numerical propagation of high energy cosmic rays in the Galaxy I: technical issues

Daniel De Marco<sup>†</sup>, Pasquale Blasi<sup>‡</sup> and Todor Stanev<sup>†</sup>

<sup>†</sup> Bartol Research Institute, University of Delaware Newark, DE 19716, U.S.A.

<sup>‡</sup> INAF/Osservatorio Astrofisico di Arcetri, Largo E. Fermi, 5 - 50125 Firenze, ITALY

E-mail: ddm@bartol.udel.edu, blasi@arcetri.astro.it,  
stanev@bartol.udel.edu

**Abstract.** We present the results of a numerical simulation of propagation of cosmic rays with energy above  $10^{15}$  eV in a complex magnetic field, made in general of a large scale component and a turbulent component. Several configurations are investigated that may represent specific aspects of a realistic magnetic field of the Galaxy, though the main purpose of this investigation is not to achieve a realistic description of the propagation in the Galaxy, but rather to assess the role of several effects that define the complex problem of propagation. Our simulations of Cosmic Rays in the Galaxy will be presented in Paper II. We identified several effects that are difficult to interpret in a purely diffusive approach and that play a crucial role in the propagation of cosmic rays in the complex magnetic field of the Galaxy. We discuss at length the problem of the extrapolation of our results to much lower energies where data are available on the confinement time of cosmic rays in the Galaxy. The confinement time and its dependence on particles' rigidity are crucial ingredients for 1) relating the source spectrum to the observed cosmic ray spectrum; 2) quantifying the production of light elements by spallation; 3) predicting the anisotropy as a function of energy.

## 1. Introduction

A complete understanding of the origin of Cosmic Rays (CRs) will be achieved when the acceleration processes, the sources and the propagation from the sources to the Earth will be included in a self-consistent theoretical framework. This goal is far from being achieved: for ultra high energy cosmic rays (UHECRs) the issue of the propagation is probably easier to understand since the effect of extragalactic magnetic field is expected to be not crucial, at least above energies of  $\sim 4 \times 10^{19}$  eV [1]. On the other hand in this case the sources are fully unknown. For CRs below  $\sim 10^7 - 10^8$  GeV we are confident that the sources are located within our Galaxy and most likely are supernova remnants (SNRs) [2]. In this respect a large bulk of information is being collected from X-ray and  $\gamma$ -ray astronomy: high resolution X-ray observations have shown the presence of intense magnetic fields in the vicinity of the shocks that bound the shell of the remnant [3], thereby making the acceleration process easier to understand. The combination with the observed X-ray spectra and the outstanding detection of 10 – 100 TeV gamma rays from a few SNRs [4] make a rather strong case in favor of these astrophysical sources being the accelerators of protons up to the knee or slightly above it [2]. Nuclei would then be accelerated to even higher maximum energies, up to  $\sim 10^{17}$  eV for iron nuclei. Although the observational situation and the theoretical understanding are both experiencing a substantial improvement as far as the sources (or at least SNRs) are concerned, a realistic description of the propagation of CRs in the interstellar medium (ISM) is still missing, despite the very impressive amount of work carried out on the topic (see [5] and references therein for a recent review). Such work may be classified in two broad classes: analytical approaches and simulations.

Most analytical work is based on the solution of the diffusion-convection equation from a distribution of sources in a medium with given diffusion properties. We include in this class the work that is based on a numerical solution of the transport equation (e.g. GALPROP [6] or the model presented in [7]). In the most general case, the equation has been solved with both parallel and perpendicular diffusion taken into account. These approaches start from the premise that the magnetic field of the Galaxy induces only a diffusive behaviour on CRs, namely the turbulent field is the key ingredient. This component is provided *a priori*, either in the form of pre-calculated diffusion coefficients or in the form of turbulent spectra. It is worth stressing that the spectrum of the turbulence responsible for particle diffusion, the total power in turbulent modes and the origin of such turbulence are unknown. However, if one assumes that the spectrum is known, then the diffusion coefficients could be calculated, at least in principle, using quasi-linear theory and neglecting the geometry of the large scale background magnetic field.

The most common approach in the literature consists of using low energy data on the ratio of secondary to primary nuclei in CRs as a function of energy to infer the energy dependence of the propagation time, which in turn leads to a rough knowledge of the energy dependence of the diffusion coefficient. Such dependence is then adopted

in the solution of the transport equation.

The shortcomings and advantages of using the diffusion equation to describe the propagation of CRs are easy to identify: this approach allows one to achieve a basic understanding of some issues (for instance the spectral steepening induced by the particle propagation and leakage from the Galaxy). Moreover the approach can be used without limitations in the dynamical range (particles from very low to very high momenta can be included). On the other hand, the diffusion coefficients are given quantities; even when the diffusion coefficients (as functions of particle momentum and spatial location) are calculated from first principles (quasi-linear theory) they are often used in regimes where the initial assumptions do not necessarily hold. In addition, a multitude of effects related to spatial gradients of the large scale fields are hardly accounted for.

The numerical simulation of the propagation of CRs in arbitrary magnetic fields solves part of these problems, but is limited by the constraints on the computational time. Previous investigations using this technique concentrated on very high energy cosmic rays ( $\sim 10^{18-19}$  eV), and on the deflections produced by their passage into the Galactic Magnetic Field [8] or on their anisotropy around  $10^{18}$  eV [9]. Other attempts investigated lower energies, e.g. Ref. [10] was able to reach down to  $10^{17}$  eV, and calculated the times of escape from the galaxy as a function of energy. The results obtained, however, seem to be inconsistent with measurements at low energy. Indeed, in Ref. [10], the escape time at  $10^{17}$  eV is found to be of the order of  $10^5$  yr with an energy dependence of  $E^{-1}$ , much steeper than the one expected for example from a normal Kolmogorov turbulence. The extrapolation of this value to  $10^9$  eV produces a value several orders of magnitude larger than the measured one. The problem of the steepness of the escape time in the simulations seems to be a general one: it is present also in our simulations and seems to continue to lower energies as we discuss below.

In this paper we describe the numerical code that we recently completed for the propagation of cosmic rays in arbitrary magnetic fields (both in their large scale and turbulent components). The code represents a substantial improvement on previous efforts in the same direction in several ways: first, we succeeded in propagating the particles down to energies of  $10^{14}$  eV, lower by at least one/two orders of magnitude compared with previous simulations. Second, the turbulence responsible for diffusive particle motion can be taken as three dimensional or one-dimensional, and as isotropic or anisotropic. The large scale field is also completely arbitrary.

We present the results of this simulation effort in two papers. In the present paper (Paper I) we discuss all technical aspects and apply the approach to several toy models of the magnetic field of the Galaxy in order to emphasize the role of the physical effects that is necessary to include in order to understand the propagation of CRs. In a second paper (Paper II) we will describe the results of the simulation for given configurations of Galactic magnetic fields which are commonly assumed as realistic.

The paper is organized as follows: In §2 we describe the technical aspects of the simulation, with special attention to the generation of the turbulent magnetic field. In §3 we illustrate some basic concepts of diffusion in the context of quasi-linear theory,

which allows us to define what is the common lore of cosmic ray propagation in the Galaxy in terms of diffusion and drifts. In §4 we describe the numerical procedure adopted to calculate the parallel and perpendicular diffusion coefficients. Finally, in §5 we describe the results of our computations for several toy models of the large scale field of the Galaxy. We present our conclusions in §6.

## 2. Description of the simulation

We propagate particles in a magnetic field,  $\mathbf{B} = \delta\mathbf{B} + \mathbf{B}_0$ , that is the sum in each point of a regular and a random component. Both of them can in principle depend on the position. As detailed in Ref. [11] there are basically two methods to implement the turbulent field: 1) pre-computing the field on a grid using Fast Fourier Transform (FFT) and 2) calculating the field in each point along the particle trajectory as the superposition of plane waves [12].

In the FFT approach the field is pre-computed on a grid in real space from its power spectrum in reciprocal space. We set up a three dimensional grid with integer coordinates from 0 to  $N - 1$ . Each vertex on the grid corresponds to a wave vector  $\mathbf{k}$  with components given by the coordinates of the vertex. If any one of the components of  $\mathbf{k}$ , for example  $k_x$ , is larger than  $N/2$ , then we substitute it with  $-(N - k_x)$  in order to take into account negative frequencies. For each  $\mathbf{k}$  we construct an amplitude vector,  $\mathbf{B}_{\mathbf{k}}$ , with a length proportional to the square root of the power in the corresponding mode:  $k^{-(\gamma+2)/2}$ , a random direction in the plane orthogonal to  $\mathbf{k}$  and a random phase. Choosing the amplitude proportional to  $k^{-(\gamma+2)/2}$  makes sure that the power spectrum of the turbulent field is  $\mathcal{P}(k) \propto k^{-\gamma}$ , whereas choosing the direction in the plane orthogonal to  $\mathbf{k}$  assures that  $\nabla \cdot \delta\mathbf{B} = 0$ . We also have to make sure that  $\mathbf{B}_{\mathbf{k}}$  satisfies the following condition for the resulting magnetic field to be real:  $\mathbf{B}_{(k_1, k_2, k_3)} = \mathbf{B}_{(N-k_1, N-k_2, N-k_3)}^*$ . The normalization is obtained by requiring that  $\langle \delta B^2 \rangle = \sum B_{\mathbf{k}}^2$  and  $B_{\mathbf{k}=(0,0,0)}$  is set to 0 to have  $\langle \delta\mathbf{B} \rangle = 0$ . At this point we compute the FFT [13] and obtain the turbulent field defined on a cubic grid with side  $L_{\max}$  and spacing  $L_{\min} = L_{\max}/N$ . We typically use  $N = 256$ .

We assume the box is replicated periodically all over the simulation volume and in order to calculate the turbulent field in a given point the code uses the field value of the closest vertex. Another possibility is to do an interpolation of the values at the eight vertexes surrounding the point. We verified that the results obtained with the two methods are equal on scales larger than the cell size ( $L_{\min}$ ) and we decided to use the former method.

The above description is valid for the general case of isotropic turbulence. We also used 1D turbulence, a superposition of Alfvén waves, and in this case the generation proceeds along the same lines, but the  $\mathbf{k}$ s are now chosen only parallel to the background field, so that the fluctuating magnetic field is always perpendicular to it. For the 1D field we typically use  $N = 4096$ .

In the second approach the field is constructed as the sum of  $N_m$  plane waves

[12, 14]:

$$\delta\mathbf{B} = \sum_{n=1}^{N_m} A_{\mathbf{k}_n} \boldsymbol{\epsilon}_n \exp(ik_n z'_n + i\beta_n), \quad (1)$$

where  $\boldsymbol{\epsilon}_n = \cos \alpha_n \hat{\mathbf{x}}'_n + i \sin \alpha_n \hat{\mathbf{y}}'_n$  and  $\alpha_n$  and  $\beta_n$  are random phases. The primed coordinates are obtained by rotating the reference frame so that the  $z$  axis coincides with the direction of propagation of the  $n$ -th wave,  $\mathbf{k}_n$ . The directions of the  $N_m$  waves are chosen randomly, while their amplitudes,  $A_{\mathbf{k}_n}$ , are chosen as a function of  $|\mathbf{k}_n|$  according to the type of turbulence wanted. We follow Ref. [12] and we use:

$$A_{\mathbf{k}}^2 = \sigma^2 G(\mathbf{k}) \left[ \sum_{n=1}^{N_m} G(\mathbf{k}_n) \right]^{-1}, \quad (2)$$

where

$$G(\mathbf{k}) = \frac{\Delta V^{(d)}}{1 + (kL_c)^{\gamma+(d-1)}}. \quad (3)$$

In these equations  $\sigma$  fixes the normalization of the field,  $\sigma^2 = \langle \delta B^2 \rangle$ ,  $L_c$  is the correlation length,  $\gamma$  is the slope of the turbulence power spectrum,  $d$  is its dimensionality and  $\Delta V^{(d)}$  is the volume element for the chosen dimensionality. In the present paper we use 3D and 1D turbulence and in these cases  $\Delta V^{(3)} = 4\pi k^2 \Delta k$  and  $\Delta V^{(1)} = \Delta k$ . The wavenumbers are chosen evenly spaced in logarithmic scale between  $k_{\min}$  and  $k_{\max}$  and  $\Delta k = k \Delta \log k$ .

The number of waves,  $N_m$ , used in the summation (1), is a key parameter and it should be large enough to reasonably describe the turbulence. In Ref. [14] it was shown that if  $N_m$  is too small the transition from rectilinear to diffusive propagation occurs on timescales much larger than the correct ones. It was also found that a value of 100 waves per decade is a reasonable compromise between accuracy and computation time and we use this value in our simulations.

The only difference for the case of 1D turbulence is that instead of choosing the  $\mathbf{k}_n$  isotropically we choose them in the direction parallel to the background field.

Both the methods described have their advantages and disadvantages: with the FFT approach the time needed to obtain the turbulent field in a given point is in general much smaller than in the plane wave approach. In the first case all that is required is a lookup in a table (and possibly some interpolations), whereas in the latter case there is a summation over hundreds of waves to be done. On the other hand, the dynamic range of the turbulence,  $L_{\max}/L_{\min}$ , in the FFT approach is limited (at least in the isotropic turbulence case) by the memory available to store the huge matrices describing the magnetic field grid, whereas in the plane wave approach the memory limitations are absent and the dynamic range can be as big as required with the only limit given by the computation time. As mentioned in Ref. [11], other limitations of the FFT approach are inherent in its discreteness,  $L_{\min}$ , and in its limited size,  $L_{\max}$ , and the results obtained with it can not be trusted when the Larmor radius of the particles is smaller than  $L_{\min}$  or larger than  $L_{\max}$ .

### 3. Basic facts about diffusion and drifts

In this section we summarize the basic facts on diffusion of cosmic rays in a turbulent magnetic field superimposed to a large scale spatially constant magnetic field  $\mathbf{B}_0 = B_0 \hat{\mathbf{z}}$ . Gradients in the large scale field induce drift motions of the particles that add to the diffusive motion and in fact in some circumstances may even dominate upon diffusion.

#### 3.1. Diffusion

In all the cases that we consider below we investigate 3D turbulence, namely the perturbation of the large scale field has components both in the plane perpendicular to  $\mathbf{B}_0$  and along  $\mathbf{B}_0$ . Therefore this case is somewhat more complex but supposedly more realistic than the simpler case of Alfvén waves propagating along the field  $\mathbf{B}_0$  (we refer to this case as the *1D case*), typically considered in the literature on quasi-linear theory. In the case of 3D turbulence, the perpendicular diffusion, though small compared with the parallel diffusion in the quasi-linear regime, may become important for the cases of strong turbulence  $\delta B/B_0 > 1$ . On the basis of quasi-linear theory the ratio of perpendicular to parallel diffusion coefficient is given by

$$\frac{D_{\perp}}{D_{\parallel}} = \frac{1}{1 + (\lambda_{\parallel}/r_L)^2}, \quad (4)$$

where the parallel pathlength is  $\lambda_{\parallel} = 3D_{\parallel}/v$ ,  $v$  is the particle velocity and  $r_L$  is the Larmor radius in the unperturbed magnetic field  $B_0$ . This expression remains valid as long as  $\delta B/B_0 \ll 1$ , but it also suggests that the perpendicular diffusion coefficient approaches the parallel diffusion coefficient in the regime of strong turbulence. In fact the real ratio of the diffusion coefficients is affected by the random walk of the field lines, which is not taken into account in Eq. 4. This fact was found in [15] and further discussed in [11] and is illustrated in the next section in detail since it plays a crucial role in the understanding of the results of the simulation of cosmic rays in the Galaxy.

The parallel diffusion coefficient can be estimated from the 1D case, by using the quasi-linear theory:

$$D_{\parallel} = \frac{1}{3} r_L c \frac{1}{\mathcal{F}(k)}, \quad (5)$$

where  $\mathcal{F}(k) = (\delta B(k)/B_0)^2$  is the normalized power in the turbulent modes with wavenumber  $k \propto 1/p$  resonant with the particles with momentum  $p$ . Even in the 3D case this is a reasonable approximation to the parallel diffusion coefficient since this is dominated by the components of the perturbing field which are perpendicular to the background field. In this case one can see that the perpendicular diffusion coefficient is

$$D_{\perp} \approx D_{\parallel} \mathcal{F}(k)^2. \quad (6)$$

Since by definition  $\mathcal{F}(k) \ll 1$  it is easy to see that  $D_{\perp} \ll D_{\parallel}$ , which implies that in most cases the effect of perpendicular diffusion is irrelevant if the propagation occurs in the regime of weak turbulence.

In numerical simulations of the propagation of cosmic rays in the Galaxy it is usually assumed that  $\delta B/B_0 \sim \mathcal{O}(1)$ . This ratio is supported by general estimates, such as equipartition, cosmic ray behavior and observations of total magnetic field in elliptical galaxies [16], rather than direct observations.

Let us assume that the measurement of the abundances of light elements and the estimate of the anisotropy of cosmic rays at low energies may be taken as realistic for the determination of the diffusion properties of the ISM.

The anisotropy of cosmic rays at low energies is observed to be at the level of  $\delta \sim 10^{-4}$ , and in the context of quasi-linear theory (QLT) it is of order  $v_D/c$ , where  $v_D$  is the drift velocity of cosmic rays in the magnetic field of the Galaxy. The condition  $v_D/c \sim 10^{-4}$  implies  $v_D \sim 3 \times 10^6$  cm/s. This is in good agreement with the theory again, because in QLT the streaming instability forces the streaming of cosmic rays to occur at bulk velocities lower than the Alfvén speed,  $v_A = B/\sqrt{4\pi\rho} \sim 2 \times 10^6$  cm/s for  $B = 3\mu G$  and gas density  $0.1\text{cm}^{-3}$  (this should be considered as an average value over the magnetized halo of the Galaxy, say within 3 kpc from the disk). In other words, the anisotropy is exactly what one would expect on the basis of bulk motion of cosmic rays at the Alfvén speed ( $v_D = v_A$ ). In QLT the pathlength for a particle to suffer a change in direction by 90 degrees is

$$\lambda = \frac{c}{\Omega \left(\frac{\delta B}{B}\right)^2} = \frac{r_L(E)}{\mathcal{F}(k(p))} \quad (7)$$

where  $\Omega = c/r_L(p)$  is the gyration frequency of the particle and  $k = 1/r_L(p)$ .

The pathlength  $\lambda$  determines the confinement time in a region of size  $L$  as

$$\tau = \frac{L^2}{c\lambda}. \quad (8)$$

From observations of the abundance of light elements this time is measured to be  $\sim 3 \times 10^6$  years, while from the abundance of unstable radioactive isotopes one gets a larger number,  $\sim 2 \times 10^7$  years [17]. These two numbers correspond respectively to  $\lambda = 10$  pc and  $\lambda = 1.5$  pc. Here we assumed that the magnetized region of the Galaxy in the direction perpendicular to the disk has a typical size  $L = 3$  kpc. Note also that rigorously we may use the parallel diffusion coefficient to estimate the escape from the disk only if the magnetic field is oriented along  $z$ , which is at odds with the conventional models of Galactic magnetic field. Therefore it is worth keeping in mind that a more realistic estimate is likely to differ from the one just illustrated and often used in the literature.

From the equation for  $\lambda$  one immediately obtains:

$$\epsilon_1 = kP(k) = \left(\frac{\delta B}{B}\right)^2 = 3.5 \times 10^{-8} \quad (9)$$

for  $\lambda = 10$  pc and

$$\epsilon_2 = kP(k) = \left(\frac{\delta B}{B}\right)^2 = 2.4 \times 10^{-7} \quad (10)$$

for  $\lambda = 1.5$  pc. For the numerical evaluation we considered cosmic rays with mean energy 1 GeV. These values of  $kP(k)$  correspond to  $\delta B/B_0 \sim 2 \times 10^{-4}$  and  $\sim 5 \times 10^{-4}$  respectively on the relevant scales. On such scales it appears that the assumptions of QLT are fulfilled.

If the power spectrum is in the form of a power law, we can write  $P(k) = P_0 \left(\frac{k}{k_0}\right)^{-\alpha}$  and limit ourselves to the two interesting cases  $\alpha = 5/3$  (Kolmogorov spectrum) and  $\alpha = 3/2$  (Kraichnan spectrum). In both these cases most power is in the form of modes with the largest spatial scale (namely at  $k_0$ , assumed here to be  $k_0 \approx 1/100$  pc). The modes of wavenumber  $k_0$  resonate with particles with energy  $E_0 = 2.8 \times 10^{17}$  eV. The propagation of particles with energies larger than  $E_0$  is described in terms of a diffusion coefficient with a steeper energy dependence than the one discussed here (Bohm diffusion) and eventually straight line propagation. From the numerical values obtained above, and assuming that  $k_0 \approx 1/100$  pc, one easily infers that the power on a scale  $k_0$  is

$$P_0 k_0 \approx \epsilon_1 \left(\frac{k(1\text{GeV})}{k_0}\right)^{\alpha-1} = 3.2 \times 10^{-3} \quad (1.8 \times 10^{-4}) \quad (11)$$

for  $\lambda = 10$  pc and  $\alpha = 5/3$  ( $\alpha = 3/2$ ), and

$$P_0 k_0 \approx \epsilon_2 \left(\frac{k(1\text{GeV})}{k_0}\right)^{\alpha-1} = 0.02 \quad (1.3 \times 10^{-3}) \quad (12)$$

for  $\lambda = 1.5$  pc and  $\alpha = 5/3$  ( $\alpha = 3/2$ ).

These estimates show that the total power in the turbulent field may be appreciably smaller than unity, which of course affects the normalization of the diffusion coefficient, the confinement time and the expected anisotropy at higher energies. The main problem with these estimates is that they are based solely upon the parallel diffusion coefficient, which, as discussed below may be incorrect. The issue of the strength of the turbulent field relative to the strength of the regular field remains therefore open.

It is worth stressing that for  $\alpha = 5/3$  the diffusion approximation is broken at  $E_{th} \approx 8 \times 10^{15}$  eV when  $\lambda = 10$  pc and  $E_{th} \approx 2 \times 10^{18}$  eV when  $\lambda = 1.5$  pc. For  $\alpha = 3/2$  we have  $E_{th} \approx 10^{14}$  eV for  $\lambda = 10$  pc and  $E_{th} \approx 6 \times 10^{15}$  eV for  $\lambda = 1.5$  pc. This implies that at energy  $E_{th}$  the anisotropy is expected to become of order unity. Among all cases considered, the only case that seems to be compatible with the fact that no large anisotropy is observed up to the knee is the case  $\alpha = 5/3$  and  $\lambda = 1.5$  pc. Note that this does not necessarily imply that a large anisotropy should be observed at  $E_{th} \approx 2 \times 10^{18}$  eV, since at this energy the chemical composition in the Galaxy is expected to be contaminated by heavy elements, which are as isotropic as the particles with energy  $E_{th}/Z$ . Despite the interesting conclusion, this has to be considered just as a hint, because of the several assumptions that enter the previous estimate (for instance the value of  $L$  and  $k_0$  and assumptions about geometry of the system).

The predicted escape time from the Galaxy as a function of energy is more solidly predicted to be  $\tau(E) \propto E^{-1/3}$  for Kolmogorov spectrum and  $\tau(E) \propto E^{-1/2}$  for Kraichnan spectrum. It is worth stressing that this simple prediction, widely used in the literature,

completely neglects the possibility of perpendicular diffusion or when it is not neglected, the assumption is adopted that the scaling with energy of the perpendicular diffusion coefficient is the same as for the parallel diffusion coefficient. Unfortunately, as we show below, the role of perpendicular diffusion in the Galaxy is likely to be crucial.

### 3.2. Drifts

Gradients in the modulus or orientation of the large scale field  $\mathbf{B}_0$  induce drift motions in the direction perpendicular to both the local field and its gradient. The drift velocity of the guiding center can be written as [18]:

$$\begin{aligned} \mathbf{V}_\perp &= \frac{cp}{ZeB_0} \left\{ \frac{1}{2} \sin^2 \alpha \frac{\mathbf{B}_0 \times \nabla B_0}{B_0^2} + \cos^2 \alpha \frac{\mathbf{B}_0 \times [(\mathbf{B}_0 \cdot \nabla) \mathbf{B}_0]}{B_0^3} \right\} \\ &= cr_L \left\{ \frac{1}{2} \sin^2 \alpha \frac{\mathbf{B}_0 \times \nabla B_0}{B_0^2} + \cos^2 \alpha \left[ \frac{\mathbf{B}_0 \times \nabla B_0}{B_0^2} + \frac{(\nabla \times \mathbf{B}_0)_\perp}{B_0} \right] \right\}, \end{aligned}$$

where  $\alpha$  is the pitch angle of the particle. The first term in this expression reflects the transverse gradient of the field strength while the second term represents the effect of the curvature of the field lines.

The above expression should be interpreted as the drift velocity averaged over a gyration period of the particle. As an estimate of the order of magnitude of the time scale for escape from the region of size  $L$  due to drift motion, we can write  $\tau_D(E) \sim \frac{L\lambda_{grad}}{cr_L(E)}$ , where  $\lambda_{grad}$  is the spatial scale on which the gradient in the magnetic field appears. This expression clearly shows that if the drifts are relevant at all this may happen only at very high energies.

Three toy models are particularly interesting as far as drifts are concerned and will be discussed in detail in §5.2, §5.3 and §5.4. Here we limit our discussion to the expected effects of drift motions. The first model (Toy model II in §5.3) has only spatially constant (in modulus) azimuthal magnetic field. In this case the field lines are simply concentric circles in  $z = \text{const.}$  planes. The only gradient is due to the curvature of the magnetic field lines and the drift velocity is given by

$$\mathbf{v}_D = E_{18} c \cos^2 \alpha \frac{\hat{z}}{\rho}, \quad (13)$$

where  $\hat{z}$  is the unit vector in the  $z$  direction,  $\rho$  is the distance (in kpc) from the center in the plane  $z = 0$  and  $E_{18}$  is the particle energy in units of  $10^{18}$  eV. Clearly this expression and the ones we will list below are valid as long as the spatial scale of the gradient is much larger than the Larmor radius of the particles. This condition also assures that the drift velocity is always smaller than the speed of light. From Eq. 13 one can see that the drift pushes the particles perpendicular to the plane.

The second toy model that we will consider is similar to the previous one but with the strength of the magnetic field having a gradient along the  $\rho$  direction (see Eq. 5.3).

It is easy to predict that also in this case the drift velocity is oriented along the  $\hat{z}$  direction. The drift velocity in this case is

$$\mathbf{v}_D = E_{18} c \frac{1}{17} (1 + \cos^2 \alpha) \hat{z} \quad \text{for } \rho > 4\text{kpc}. \quad (14)$$

Finally, in the third toy model we assume that the magnetic field is still azimuthal but is constant in the  $z = 0$  plane and has a gradient in the  $\hat{z}$  direction (see Eq. 5.4). In this case the drift velocity is

$$\mathbf{v}_D = E_{18} c \left[ \cos^2 \alpha \frac{1}{\rho} \hat{z} + \sin^2 \alpha \frac{1}{2z_c} \hat{\rho} \right] \exp(z/z_c). \quad (15)$$

Clearly in this third case the direction of the drift is no longer along  $\hat{z}$  and depends on  $\rho$ .

#### 4. Determination of the parallel and perpendicular diffusion coefficients

To calculate the diffusion coefficients we inject a few thousand particles of a given energy isotropically in a magnetic field composed of a constant regular component along  $\hat{z}$  plus a uniform turbulent component. We record the particle trajectories and we then calculate the instantaneous parallel and perpendicular diffusion coefficients as:

$$D_{\parallel}(\tau) = \frac{\langle \Delta z^2 \rangle}{2\tau} \quad \text{and} \quad D_{\perp}(\tau) = \frac{\langle \Delta x^2 \rangle}{2\tau} = \frac{\langle \Delta y^2 \rangle}{2\tau}. \quad (16)$$

We plot the instantaneous diffusion coefficients as a function of propagation time in Fig. 1 for the case  $\delta B/B_0 = 1$ . The left panel is the parallel diffusion coefficient while the right one is the perpendicular diffusion coefficient. The parallel instantaneous diffusion coefficient increases linearly in the beginning when the particles are still only feeling the regular field and at some point flattens when the full diffusive regime is reached, typically within a few scattering lengths. In the perpendicular case the instantaneous diffusion coefficient increases for a time  $\tau_L/2 \simeq \pi \times r_L/c$ , corresponding to half a gyration around the regular field. At this point continuing the gyration the particle is going back to its starting position and the diffusion coefficient is decreasing, having a minimum at  $\tau_L$ . After some time the diffusion regime is reached and the curve shows a plateau. This plateau identifies the diffusion coefficient and we use the average of the last 15 points (the gray region in the plots) to estimate it.

In the following few paragraphs we present our results for the diffusion coefficients as a function of energy for some interesting configurations.

##### 4.1. The case of vanishing regular field

Without a background field the only type of turbulence that can be considered is isotropic turbulence. In Fig. 2 we plot the diffusion coefficient as a function of energy for 3D turbulence in a configuration with no regular field, but only turbulent field with  $L_{\text{max}} = 100 \text{ pc}$  and  $\delta B = 100 \mu\text{G}^{\ddagger}$ .

$\ddagger$  Please note that here and in the following when denoting  $\delta B = 100 \mu\text{G}$  we actually mean:  $\sqrt{\langle \delta B^2 \rangle} = 100 \mu\text{G}$ .

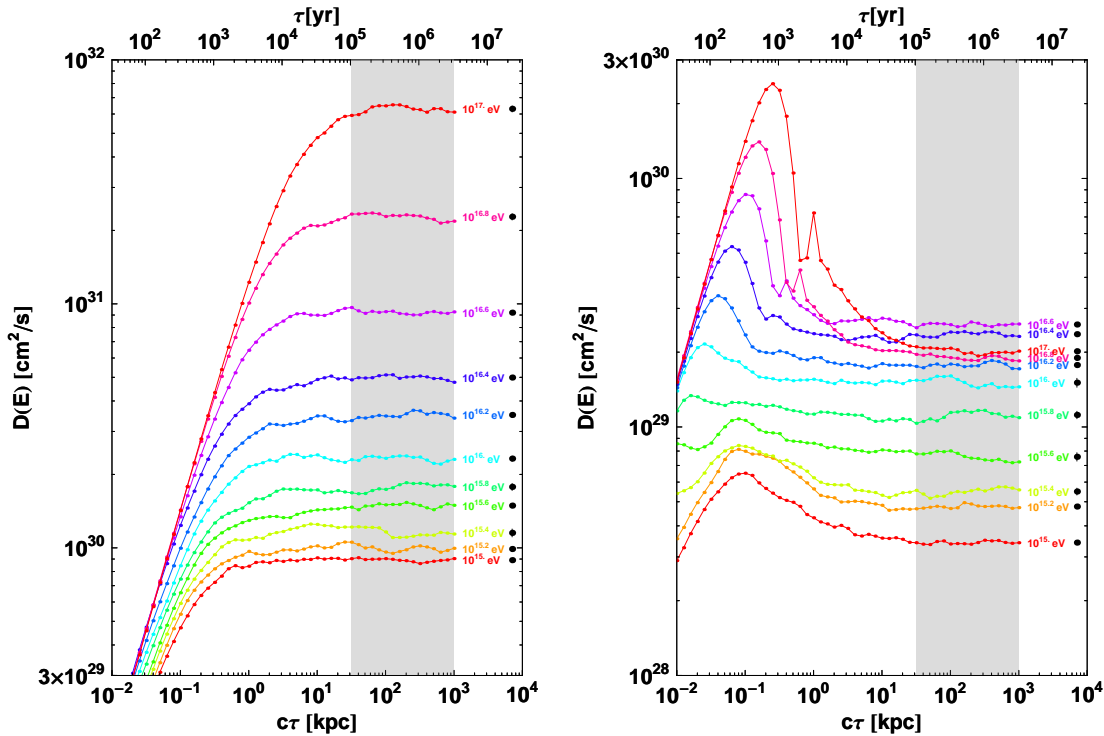


**Figure 1.** Instantaneous diffusion coefficients as a function of propagation time. Left: parallel, right: perpendicular. Each line/color corresponds to a different particle energy as indicated in the plot. The black points on the far right of each line indicate the average of the corresponding points in the gray region and they represent the estimate of the diffusion coefficient at the corresponding energy. Note the different scales on  $y$ -axes.

In this case, in order to compare our results with the ones of Ref. [14], we calculated the diffusion coefficients using 6 in the denominator of Eq. (16) instead of 2. In Fig. 2 the gray points and lines are the diffusion coefficients along the three axes, the red points are the total diffusion coefficient and the black line is the parametrization of the diffusion coefficient given in Ref. [14] that was obtained from simulations using the plane wave approach. In this case we used the FFT approach and the agreement is very good.

#### 4.2. Combination of regular and turbulent fields

In this case we use a superposition of a constant background field and a turbulent field with three levels of isotropic turbulence:  $\delta B/B_0 = 0.5, 1, 2$ . The maximum scale of the turbulence is set to  $L_{\max} = 0.1$  kpc,  $B_0 = 1 \mu\text{G}$  and we use the FFT approach to generate the turbulence. We plot the parallel and perpendicular diffusion coefficients in Fig. 3. The top three lines represent the parallel diffusion coefficients, while the bottom three the perpendicular ones. The turbulence level is given by the numbers attached to the curves. It is interesting to note that while the low energy ( $10^{15}$ -  $10^{16}$  eV) slope of the

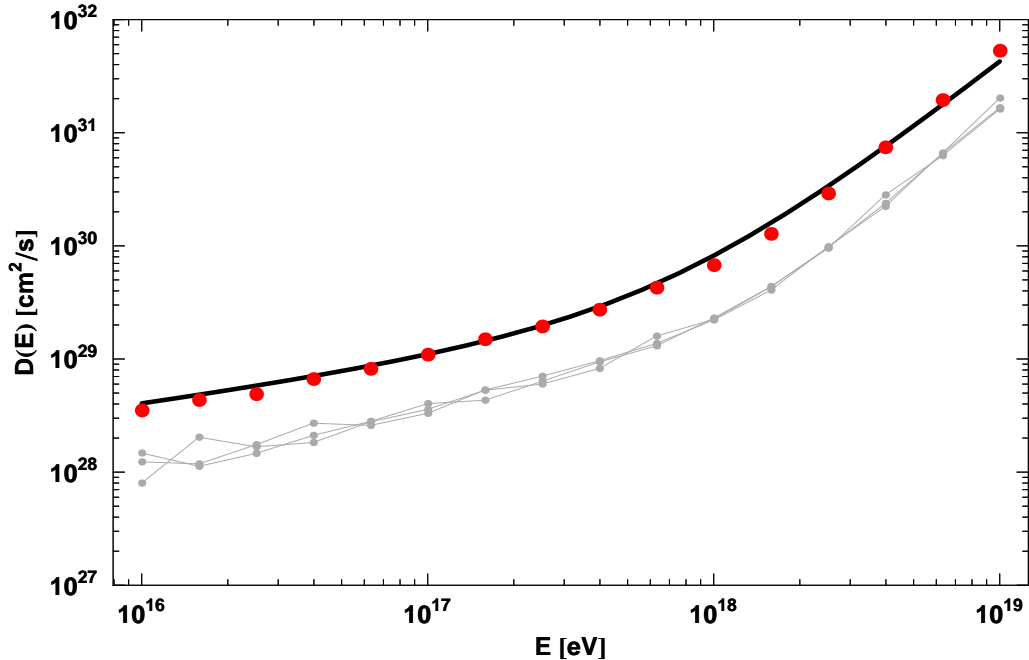


**Figure 2.** Diffusion coefficient for a configuration with vanishing regular field. The gray points and lines are the diffusion coefficients along the three axes, the red points are the total diffusion coefficient and the black line is the parametrization of the diffusion coefficient given in Ref. [14].

parallel diffusion coefficient is  $1/3$  as one would expect, the slope of the perpendicular one is steeper, being about  $0.5 - 0.6$ .

In Fig. 4 we plot the ratio of the perpendicular to parallel diffusion coefficients,  $D_{\perp}/D_{\parallel}$ , as a function of energy. The three sets of points connected by solid lines are the results of the three simulations shown in the previous plot. We compared our results with the ones obtained in Ref. [11]. The thin black lines are the results from their Fig. 6 for the cases  $\eta = 0.46$  and  $0.21$  that correspond to  $\delta B/B_0 = 0.92$  and  $0.52$  respectively. The agreement between the two sets of results is pretty good, especially for the case  $\delta B/B_0 \simeq 1$ . The ratio of the diffusion coefficients is almost constant with a slow  $E^{(0.1-0.2)}$  energy dependence.

The tiny difference in slope between  $D_{\perp}$  and  $D_{\parallel}$  at low energy is more apparent in this plot. It is interesting to note that this difference seems to be present also in the results of Ref. [11], at least for the case  $\delta B/B_0 \simeq 1$ . In the case  $\delta B/B_0 \simeq 0.5$  the scattering of their points is too big to allow for inferring any conclusions in this respect. In order to confirm that this slope was not a systematic effect due to the method used to generate the turbulence, we performed a simulation using the plane wave approach to generate the field. These results are represented by the brown dashed line. The simulation parameters and the shape of the turbulence spectrum in this case are a bit different from the others, and the resulting curve does not coincide with the one obtained from the FFT approach, but also in this case the ratio is not constant at low energy and presents a small positive slope.

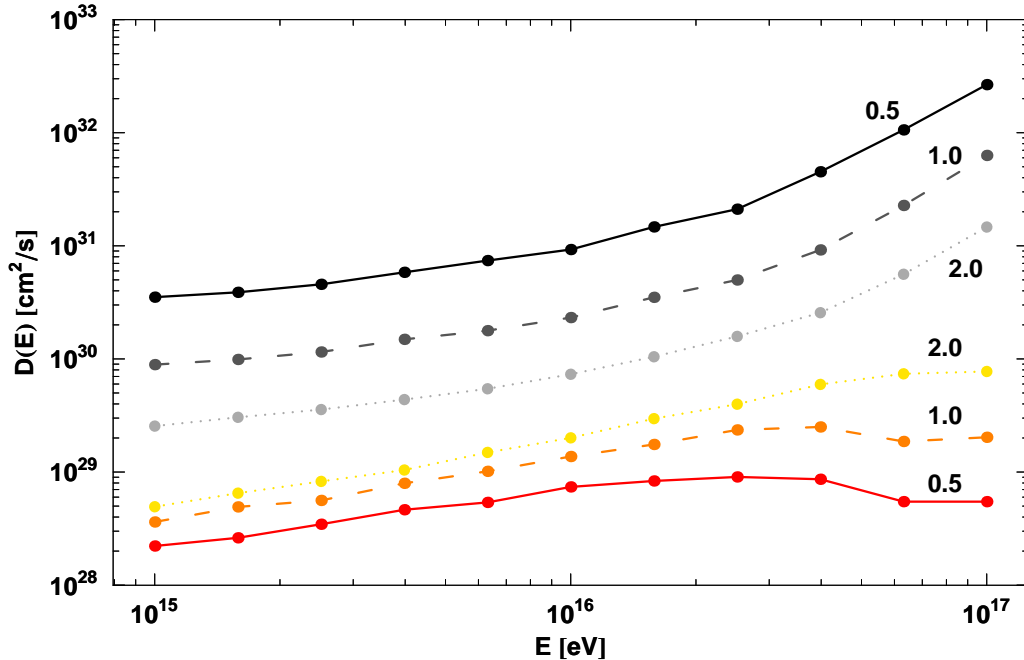


**Figure 3.** Parallel and perpendicular diffusion coefficients as a function of energy for three levels of turbulence. The upper three lines are the parallel diffusion coefficients, while the bottom three represent the perpendicular one. The level of turbulence,  $\delta B/B_0$  is given by the numbers attached to the lines.

The results of Ref. [12] show no dependence of the ratio  $D_{\perp}/D_{\parallel}$  on energy and for  $\delta B/B_0 = 1$  their result is smaller than ours by about a factor 2.

## 5. Toy models of the Galactic magnetic field

The large scale structure of the Galactic magnetic field is likely to be complex, as made of spiral arms and various types of gradients along the radial direction in the disk and along the  $\hat{z}$  axis, perpendicular to the disk. The same presence of the spiral arms induces gradients on different spatial scales. On top of this large scale structure a turbulent component is present which turns out to be responsible for the diffusive motion of cosmic rays. In all cases presented below, the values of the quantity  $\delta B/B_0$  is assumed to be spatially constant (in other words the turbulent field is a constant fraction of the large scale field). It appears rather unrealistic that the naive expectations based on quasi-linear theory may find an easy confirmation with this complex structure of the magnetic field and indeed we confirm that this is in general not the case. In order to understand the various reasons why the expectations of QLT may be not fulfilled, in the following we discuss in detail four toy models of the magnetic field of the Galaxy in both its regular (large scale) and turbulent components. The first model is that of a magnetized homogeneous sphere with only turbulent field. In this case QLT cannot even be applied because of the absence of a regular field which does not allow to develop a perturbative approach to particle propagation. In this case however the confinement

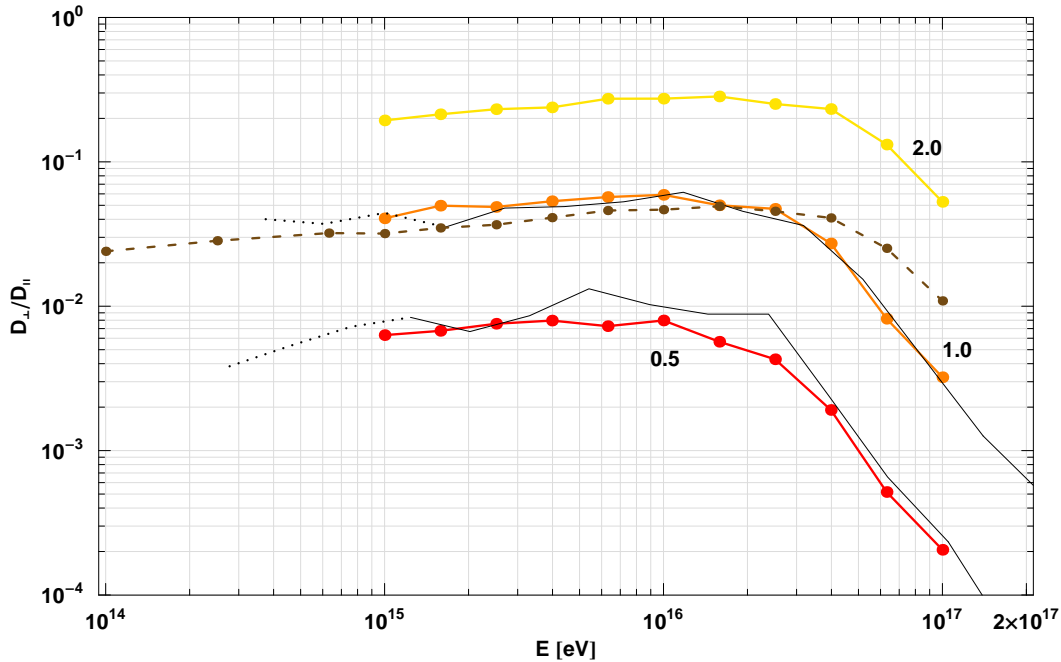


**Figure 4.** Ratio of the perpendicular to parallel diffusion coefficients,  $D_{\perp}/D_{\parallel}$ , as a function of the energy. The three set of points connected by solid lines are the results for the three levels of turbulence indicated. The points connected by the dashed line are the result of a simulation with a set of parameters similar to the one used for the orange one, but in this case using the plane waves approach instead of the FFT one. The two black thin lines are the results of Ref. [11] for  $\delta B/B_0 = 0.92$  (upper one) and  $0.52$  (lower one).

time that is obtained from simulations is close to the naive extrapolation of QLT to a regime in which it should not be applied.

The second toy model consists of a purely azimuthal, spatially constant magnetic field. The particles are injected at the position of the Earth and collected on the surface of a cylinder of radius 10 kpc and height 0.5 kpc.

The third and fourth toy models are variations of the previous one with the addition of gradients along the radial direction and along the  $z$  direction.

### 5.1. Toy model I: a magnetized homogeneous sphere

We consider a sphere filled uniformly with isotropic turbulent field with  $L_{\max} = 0.1$  kpc and  $\delta B = 0.5, 1, 2 \mu\text{G}$ . We inject protons in the center of the sphere and we collect them when they reach a distance of 2 kpc from the center. The times of escape from the sphere are plotted as triangles and boxes in Fig. 5. We also plotted, with stars, the results obtained using  $L_{\max} = 1$  kpc instead of  $L_{\max} = 0.1$  kpc for the case  $\delta B = 1 \mu\text{G}$ . The black lines are the expected propagation times obtained using the parametrization of the diffusion coefficient given in [14] and already used in §4.1 for comparison:

$$\tau(E) = \frac{R^2}{6D(E)}. \quad (17)$$

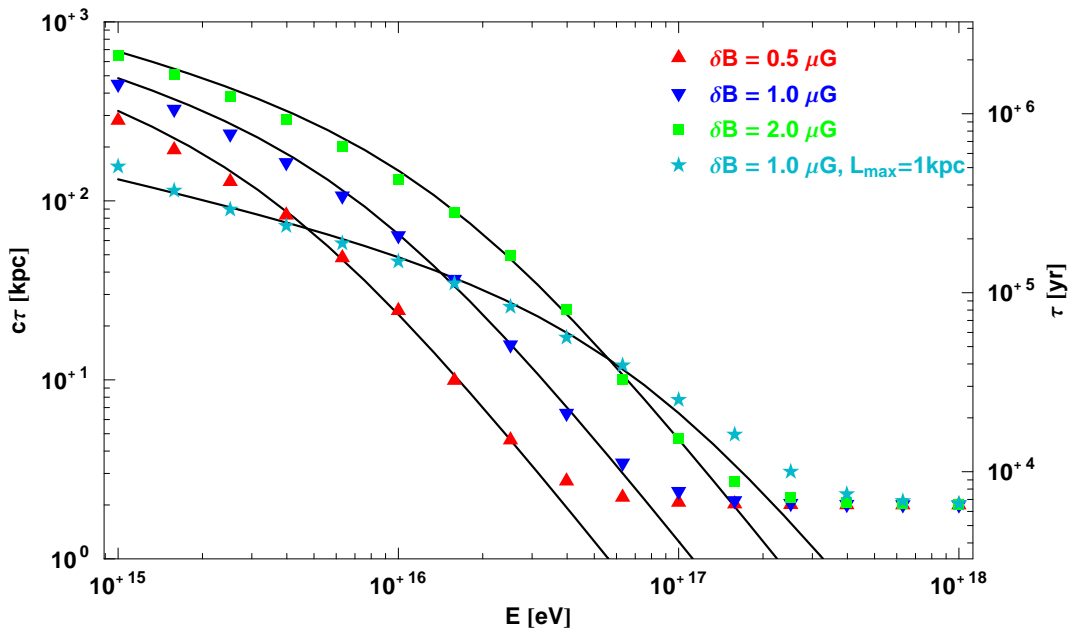


**Figure 5.** Times of escape from a sphere filled with uniform turbulent field for protons injected in the center. The levels of turbulence are indicated in the plot. The first three cases are for  $L_{\max} = 0.1$  kpc, while the last one for  $L_{\max} = 1$  kpc. The black lines are the expected results obtained using the diffusion coefficient given in Ref. [14].

The agreement is very good both in the low energy and in the transition region. Going to very high energies, the transition to straight line propagation becomes visible.

### 5.2. Toy model II: large scale azimuthal field with no spatial gradients

The magnetic field as seen from above the disk is as shown in Fig. 6. This field structure is assumed to resemble at least qualitatively the spiral structure of the Galactic field. In passing we notice that this purely azimuthal field has also recently been adopted by [19]. The turbulent field is assumed to have a Kolmogorov spectrum with a largest scale  $L_{\max} = 0.1$  kpc and total power  $\delta B/B_0 = 0.5, 1$  and  $2$ . Particles are injected at the Earth, located at  $R_{\odot} = 8.5$  kpc from the center and propagated backwards in time until they escape the cylinder of radius  $R = 10$  kpc and height above and below the disk of  $0.5$  kpc. A crucial point to realize here is that the magnetic field lines are closed loops: the magnetic field strength is spatially constant but the orientation of the field changes as illustrated in Fig. 6. The fact that the field lines are closed implies a straightforward but important conclusion: the particles cannot escape the cylinder by diffusing parallel to the magnetic field lines. The only way particles can escape is by diffusing and drifting perpendicular to the field lines, which is clearly made more difficult by the smallness of the perpendicular diffusion coefficient (see §4) as compared with the parallel diffusion coefficient. The escape times of cosmic rays as functions of energy for the various cases that have been calculated are illustrated in Fig. 7 (top

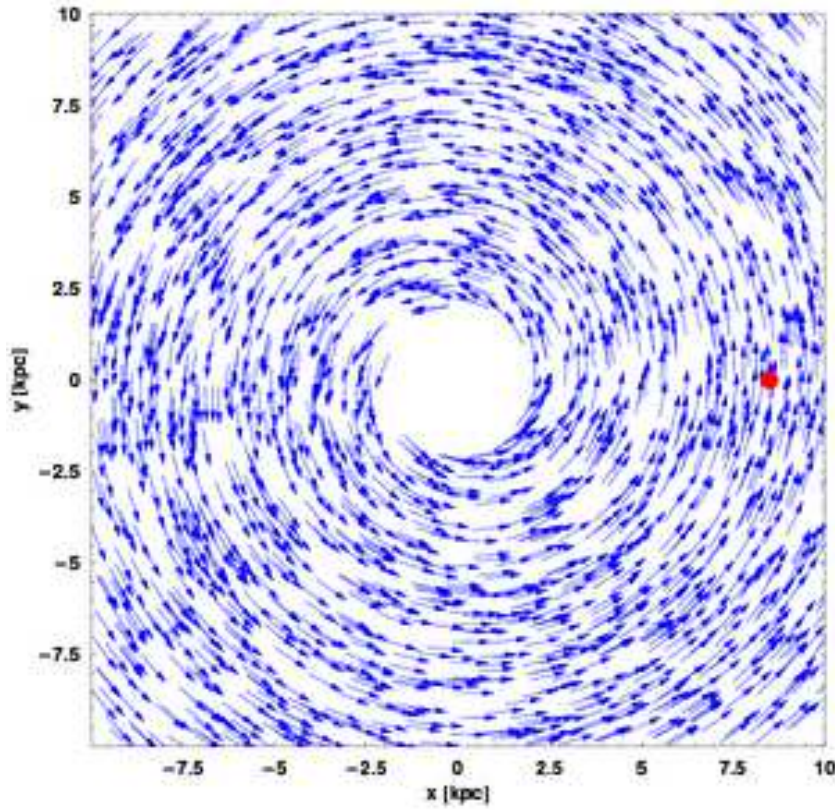


**Figure 6.** Azimuthal magnetic field in Toy model II.

panel). The lower panel of the figure illustrates the column densities experienced by cosmic rays with given energy. The gas density has been assumed to be constant and equal to  $1 \text{ cm}^{-3}$  inside the disk ( $|z| < 200 \text{ pc}$ ) and  $0.01 \text{ cm}^{-3}$  outside the disk. The different symbols refer to the values of  $\delta B/B_0$  as indicated in the figure. The straight line represents the drift time calculated from Eq. (13) using the average drift velocity. It is worth noticing that the actual drift times have a very extended tail towards large times, due to the dependence of this quantity on the angle of injection of the particles with respect to the large scale local field. The black lines and dots are the diffusion time scales,  $\propto D_{\perp}(E)^{-1}$ , where the perpendicular diffusion coefficient is taken from the simulations described in §4.

A general comment about the relative role of parallel and perpendicular diffusion is in order: parallel diffusion is more effective than perpendicular even in the case of strong turbulence considered here, but it only leads to motion of the particles along the closed magnetic field lines. Perpendicular diffusion, though much slower, is responsible for particle escape in the direction perpendicular to the disk (there is also some escape from the sides of the cylinder but this process is less efficient because the sides are  $\sim 1.5 \text{ kpc}$  away from the location of the Earth, while the halo has been assumed to be only  $0.5 \text{ kpc}$  thick). The parallel with the Galaxy is very instructive in this instance: particles diffuse effectively along the spiral arms, whose length is roughly  $R_{arm} \sim \pi R_{\odot} \sim 30 \text{ kpc}$

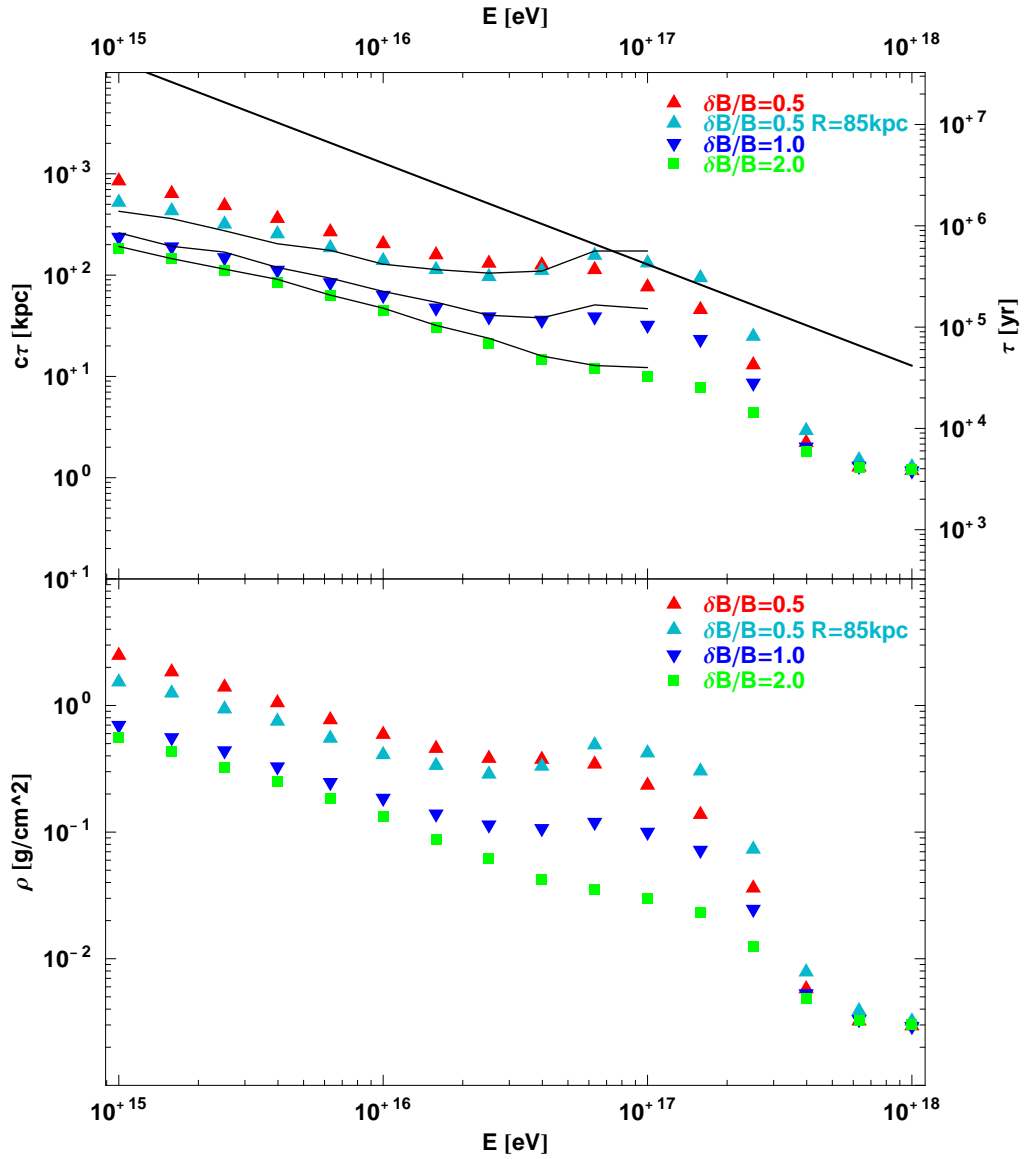


**Figure 7.** Particle escape times for Toy Model II. The upper panel shows the times required for the particles to escape from a cylinder with half-height of 0.5 kpc. The lower panel shows the grammage of gas crossed. The boxes and triangles are the values for different levels of turbulence as indicated in the plot. The injection is set at 8.5 kpc for all cases except for the light blue upward triangles for which it is set at 85 kpc. The thick black line is the drift timescale while the thin black curves represent the diffusion timescales.

long (at the distance of the Sun from the galactic center). The diffusion time parallel to the arms is therefore  $\tau_{\parallel} \sim R_{arm}^2/D_{\parallel}$ . At the same time, cosmic rays diffuse in the direction perpendicular to the disk in a time  $\tau_{\perp} \sim R_H^2/D_{\perp}$ . The ratio of the two time scales is  $\tau_{\parallel}/\tau_{\perp} \sim 10^3 D_{\perp}/D_{\parallel}$ , where we assumed  $R_H \sim 1$  kpc. For  $\delta B/B_0 \sim 1$  the perpendicular diffusion coefficient is not much smaller than  $D_{\parallel}$ , so that it is easy to understand that perpendicular diffusion may become the dominant channel of cosmic ray escape from the Galaxy rather than parallel diffusion. In our toy model this situation is extreme in that the magnetic field lines are closed and no escape at all is possible along the field. As a consequence, the energy dependence which is illustrated in Fig. 7 reflects the energy dependence of the perpendicular diffusion coefficient, which in the relevant energy range can be approximated as  $D_{\perp} \propto E^{0.5-0.6}$ . It is instructive that such a slope, usually associated (at low energies) to a Kraichnan spectrum of turbulence (parallel diffusion) can in fact be achieved with a Kolmogorov perpendicular diffusion (at least in the high energy range we are able to treat here).

The important role of perpendicular diffusion in determining the escape time is also shown by the absolute normalization of the curves in Fig. 7. For parallel diffusion, at least in the quasi-linear regime, one expects the diffusion coefficient to decrease while increasing  $\delta B/B_0$ , so that the escape times increase. In our toy model the perpendicular diffusion coefficient in fact increases with increasing  $\delta B/B_0$ .

Aside from diffusion, the escape times are also affected by drift motions. In particular, drifts become important where the drift time (the straight line in Fig. 7) becomes of the same order of magnitude of the diffusion times (black lines). For  $\delta B/B = 0.5$  this happens at energies around  $10^{17}$  eV, while drift seems irrelevant for stronger levels of turbulence. Besides this effect, which is rather clear from Fig. 7, there is a more subtle effect induced by drifts, which is evident in the low energy part of the curve for  $\delta B/B_0 = 0.5$ . One can notice that the black line illustrating the effect of diffusion (for  $\delta B/B_0 = 0.5$ ) lies below the upward red triangles obtained in the simulation. In order to understand the reason for this apparent problem, we calculated the escape times in the case in which the Earth is located at 85 kpc from the center instead of 8.5 kpc. In this case the cylinder is larger but it has the same height. But more important the curvature of the magnetic field lines is reduced appreciably so that the drift velocity drops correspondingly. One can see that the low energy behaviour in this case (upward light blue triangles) agrees well with the black curve, therefore confirming that the reason for the slim disagreement has something to do with the curvature of the field lines.

To achieve a better understanding of the modifications the drifts produce to the diffusion process we calculated the diffusion coefficients in this geometry and we found that the drifts are modifying the two perpendicular diffusion coefficients reducing the one along  $z$  and increasing the one along  $\rho$ . In fact one should keep in mind that the concepts of parallel and perpendicular diffusion were introduced here with reference to the specific case of a large scale coherent background field, with no intrinsic curvature of the field lines. When the field lines are curved, then the definition itself of parallel

and perpendicular diffusion changes, as discussed in detail in Appendix A.

At energy  $\sim 10^{17}$  eV the Larmor radius of the particles equals the maximum wavelength in the power spectrum of the turbulent field and the diffusion regime changes, gradually shifting toward the straight line propagation, which in Fig. 7 corresponds to the extreme right, flat part of the curves for the escape time. It is worth reminding the reader that all these considerations remain valid for heavier nuclei once the energy is substituted by rigidity.

We conclude this discussion of the second toy model with a comment on the absolute magnitude of the escape time. Though keeping in mind that this is a toy model of the magnetic field of the Galaxy, we believe that some qualitative conclusions can be drawn. At energy  $10^{15}$  eV the escape time for the cases considered here is  $\tau_{15} \approx 0.5 - 5$  million years (the halo height here is only 0.5 kpc). These numbers are of the same order of magnitude of the confinement times estimated from the abundance of light element in the *GeV* region, which means that in order to fit these observations one should postulate that the escape time below  $10^{15}$  eV should be practically energy independent. We could not envision any realistic mechanism able to justify such an expectation. It follows that within the limitations of the toy model 2 it is very hard to obtain a realistic, even qualitative, description of what is observed in the Galaxy at much lower energies. This conclusion is confirmed also by the curves on the grammage: at  $10^{15}$  eV cosmic rays traverse a column density of  $1 - 2 \text{ g cm}^{-2}$ . As we discuss below, this conclusion is the same for the other toy models considered here.

### 5.3. Toy model III: large scale azimuthal field with spatial gradient along $\hat{\rho}$

The global structure of the large scale azimuthal field is not changed with respect to Toy Model II, but we introduce here a gradient of the modulus of the large scale field with the radial coordinate  $\rho$  measured in the  $x - y$  plane. The radial dependence of the field is assumed to be in the form:

$$B(\rho) = \begin{cases} 2.125\mu G & \rho < 4 \\ 8.5\mu G \rho^{-1} & \rho > 4 \end{cases} ,$$

where  $\rho$  is the radius in cylindrical coordinates in units of kpc. As discussed in §3.2, in this case the drift velocity is still oriented in the  $\hat{z}$  direction, therefore the drift due to a gradient of the strength of the field behaves qualitatively as the gradient due to the curvature in the field lines, discussed in the section above. The escape time and the grammage for this case are illustrated in Fig. 8, where the red dashed line indicates the drift timescale, again calculated using the average drift velocity. At the distance of the Earth the gradient due to the radial dependence reduces the drift time by roughly a factor 2, thereby making the line for the drift time scale almost touch the red triangles ( $\delta B/B_0 = 0.5$ ). For stronger levels of turbulence the drifts become basically irrelevant, even at the highest energies. The absolute normalizations of the time scales are affected very little by the radial gradient of  $\mathbf{B}$ , therefore most comments made for Toy Model 2 are valid here too.

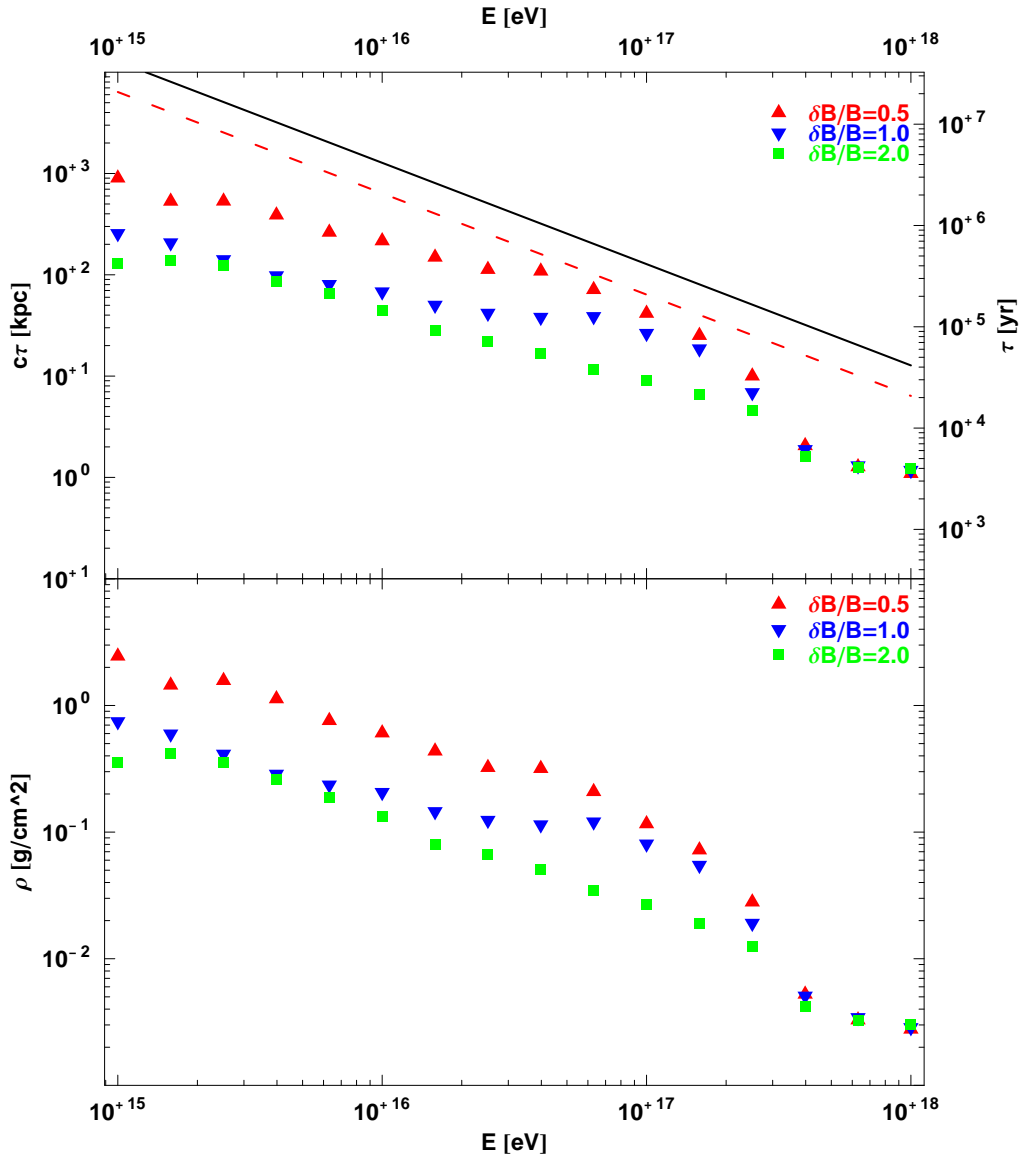


**Figure 8.** Particle escape times for Toy Model III. The black line is the drift timescale for the field of Toy Model II, while the red dashed line is the drift timescale for the present configuration.

#### 5.4. Toy model IV: large scale azimuthal field with spatial gradient along $\hat{z}$

We conclude this section by investigating the case of an azimuthal field with a gradient along  $\hat{z}$ , as described by the following expression:

$$B(z) = \exp(-z/z_c)\mu G,$$

with  $z_c = 0.25$  kpc or  $0.1$  kpc. In this case the drifts due to the  $z$ -dependence are in the radial direction and, at the Earth position, are bigger than the drifts due to the curvature of the field lines. The sum of the two drifts tends to push the particles toward

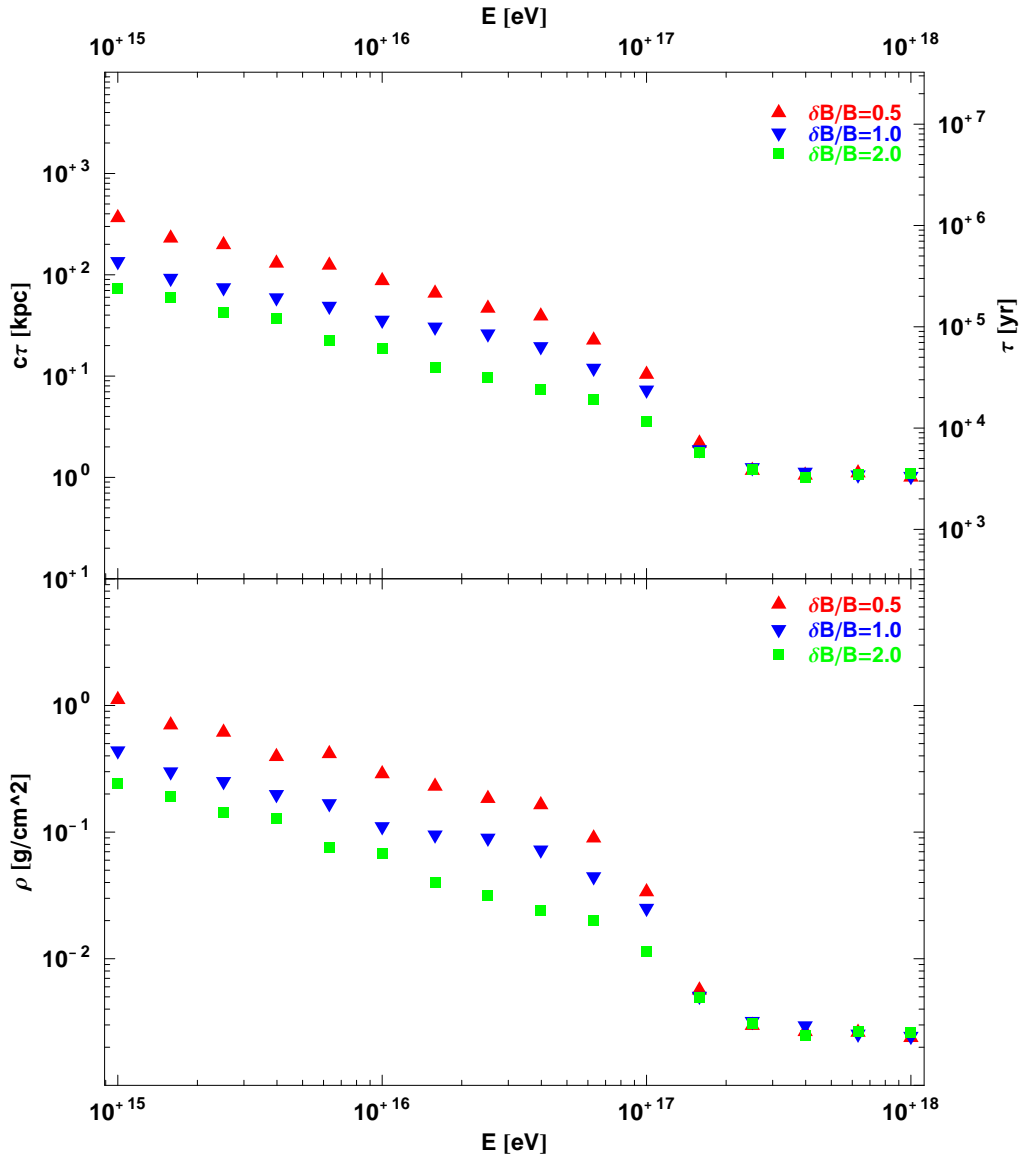


**Figure 9.** Particle escape times for Toy Model IV and  $z_c = 0.25$  kpc.

the center of the Galaxy, where the drifts due to curvature dominate. The exit points of the particles in this case are shifted in the direction of the galactic center, while in the previous two Toy Models most particles escaped from a ring with  $\rho \sim 8.5$  kpc.

The escape times and grammage for  $z_c = 0.25$  kpc are illustrated in Fig. 9 with the usual meaning of the symbols.

The effect of drifts, combined with the smaller effective size of the magnetized halo along  $\hat{z}$ , contribute to reduce the escape times. At  $10^{15}$  eV the escape time is always shorter than 1 million year. However the slopes of the curves, although rather uncertain, do not seem to point toward any flattening that may help reconcile the grammage at

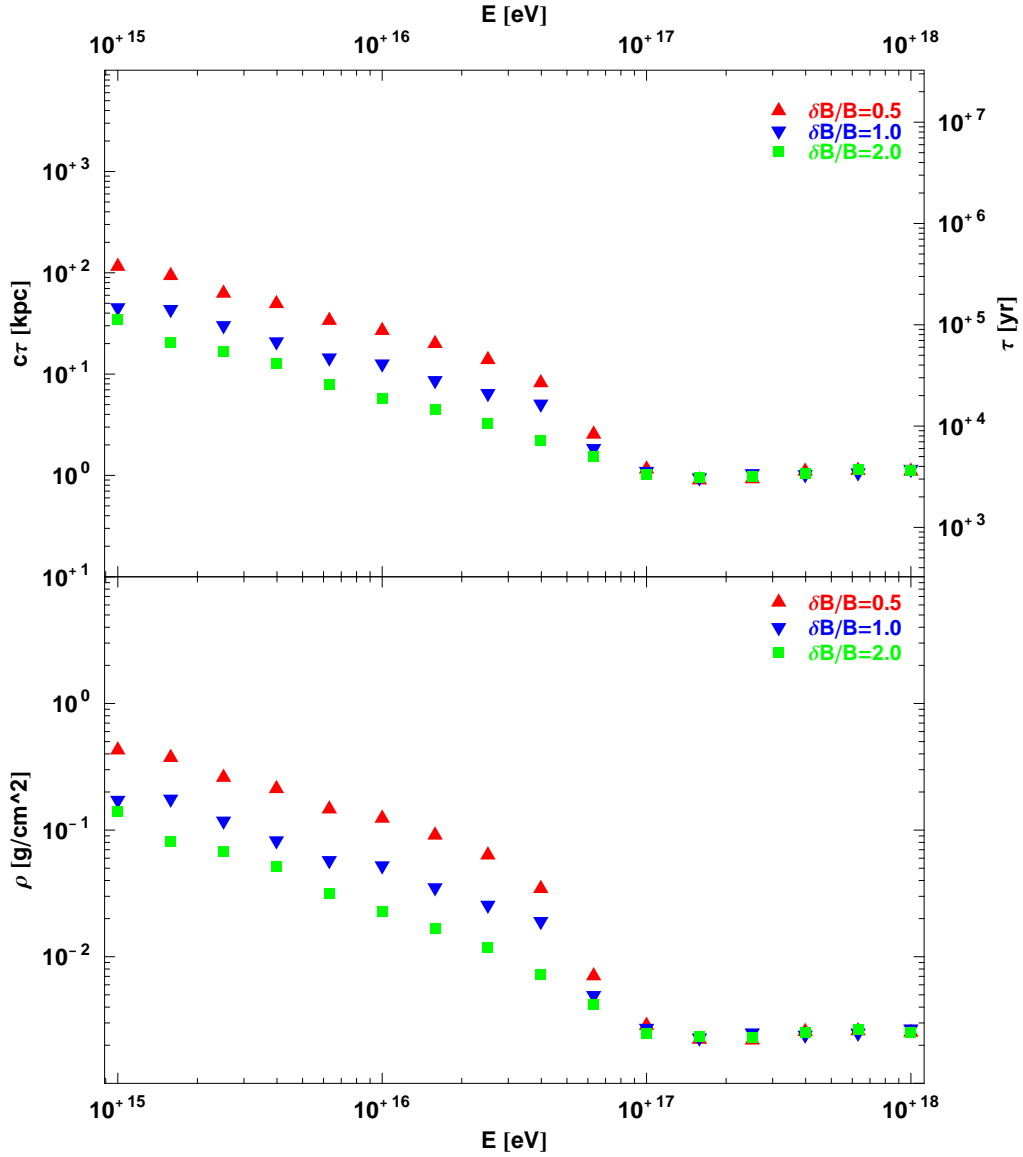


Figure 10. Particle escape times for Toy Model IV and  $z_c = 0.1$  kpc.

$10^{15}$  eV ( $0.2 - 1 \text{ g cm}^{-2}$ ) with that observed in the GeV region. A further reduction of the escape times is achieved by reducing the scale  $z_c$ . For instance the time scales and grammage for  $z_c = 0.1$  kpc are illustrated in Fig. 10.

## 6. Discussion and Conclusions

The propagation of cosmic rays in the Galaxy still presents us with numerous open questions. The standard lore goes as follows: if the sources of galactic cosmic rays (possibly but not necessarily supernova remnants) inject a spectrum  $Q(E) \propto E^{-\gamma}$  with

$\gamma \approx 2.1 - 2.4$ , then diffusion of these cosmic rays in the magnetic field of the Galaxy leads to an equilibrium spectrum which is  $n(E) \propto E^{-\gamma-\delta}$ , where the diffusion coefficient is taken in the form  $D(E) \propto E^\delta$ . For a Kolmogorov spectrum of magnetic fluctuations  $\delta = 1/3$ , while for a Kraichnan spectrum  $\delta = 1/2$ . Of course these statements apply at energies lower than the maximum energy of the accelerated particles, which for protons is expected to be  $\sim 10^{15} - 10^{16}$  eV. However, if the maximum energy of the accelerated particles were much larger, in principle the same conclusions would extend up to the energy for which the Larmor radius equals the coherence scale of the field, which is typically taken to be  $\sim 100$  pc. This corresponds to energy  $\sim (1 - 3) \times 10^{17}$  eV for a magnetic field  $1 - 3\mu G$ . The simulations illustrated in this paper can be performed for proton energies  $E > 10^{15}$  eV (in a few cases  $E > 10^{14}$  eV), therefore for at least two decades in energy we should be able to test the standard lore sketched above. We confirm that this is the case by considering a toy model with only a turbulent field with given power spectrum, in which case we are in perfect agreement with the expectations. The problems arise as soon as any complication is added to this simple scenario. We illustrate our points by considering other three toy models, each having a specific feature which is supposed to be resemblant of a corresponding feature expected to be present in the actual Galactic magnetic field. In particular we consider a benchmark situation in which the Galactic field is taken to have a perfectly azimuthal geometry, so that the magnetic field lines are closed loops. We showed how in such a geometry the role of perpendicular diffusion in the escape of particles from the toy Galaxy is crucial and leads to escape times which are too long to be reconciled with the observed confinement times at much lower energies. This conclusion should remain valid in the case in which the magnetic field lines follow the spiral arms rather than being closed, since the arms are in any case much larger in length than the size of the halo.

An important piece of information should be added: the escape times that we plotted throughout the paper are all meant to be the average of the log of the escape times. The spread around these mean values are very large, covering about one order of magnitude. Such spreads do not reflect limitations in the statistics of the propagated particles: they are rather stable if the number of particles is increased. The fluctuations are due to the several possible histories that may characterize the propagation of cosmic rays in the Galaxy. On the other hand, the mean values used to infer our conclusions are very stable.

Another important ingredient of the magnetic field configuration with closed magnetic field lines consists of the drift motions induced on the particles by the gradients in the direction of the local large scale field. The effect of drift is especially evident for high energies and low levels of turbulence. Similar drifts are introduced by gradients in the  $z$  and  $\rho$  directions.

The most important conclusion that we could achieve is that the dominant role of the perpendicular diffusion in a geometry with a prominent azimuthal magnetic field makes the expectation of the common lore hard to realize. The energy dependence of the perpendicular diffusion coefficient is not the same as that of the parallel diffusion

coefficient: more specifically in the lower energy regime it scales as  $D_{\perp} \propto E^{0.5-0.6}$ , rather than  $E^{1/3}$  as would be expected for a Kolmogorov spectrum. Unfortunately we are not able to follow this behaviour down to energies below  $10^{15}$  eV. In any case, at  $\sim 10^{15}$  eV, the escape times that we *measured* in the simulation are always too large to be extrapolated down to the few million years inferred from the abundance of light elements in the GeV energy region, even admitting that a flattening to a behaviour  $\propto E^{-1/3}$  of the escape times could be achieved below  $\sim 10^{15}$  eV.

It is interesting to speculate about possible physical effects that might cause the escape time to be reduced. From the discussion above, it is clear that reducing the level of turbulence (namely the value of  $\delta B/B$ ) does not help, since this would cause the perpendicular diffusion to decrease, thereby increasing the escape times even more. Making the halo have a smaller scale height does help, but it appears rather unrealistic to reduce this scale below 0.5 kpc (observations of the radio background from synchrotron emission of relativistic electrons hint to a typical scale height of a few kpc [20]). One possibility that we will discuss more quantitatively in Paper II is that of a galactic wind, possibly injected by cosmic rays themselves: in this case, in addition to the diffusive motion, particles would have a systematic drift velocity pushing them away from the disc of the Galaxy. If the typical wind velocity is  $u_W \sim 10^7 \text{ cm s}^{-1}$  [21], then the typical escape time due to advection is of order 5 million years, independent of momentum. It is important to notice that for the diffusion coefficients used in the literature (in the common lore usually one does not distinguish between parallel and perpendicular) this is roughly the escape time scale for cosmic rays in the GeV energy region, therefore the effect of the wind is usually relevant only for low energy particles (at higher energies the escape is dominated by diffusion). In the scenarios that we find, escape is due to perpendicular diffusion, and takes place on much longer time scales as we have seen, therefore the effect of the wind can be that of producing a roughly energy independent escape time of the order of  $\sim 5$  million years. Unfortunately this does not appear to be the correct, or at least the complete, picture either. In fact the escape time is observed to be a function of energy  $\tau \propto E^{-0.6}$ , as shown by the energy dependence of the secondary to primary ratio (e.g. [22]), although these measurements have so far been carried out only up to energies of the order of  $10^4 - 10^5$  MeV/nucleon.

## Acknowledgments

T.S. and D.D.M. wish to acknowledge useful discussions with Randy Jokipii, Joe Giacalone and Bill Matthaeus. The work of D.D.M. and T.S. is funded in part by NASA APT grant NNG04GK86G. The work of P.B. is partially funded through grant PRIN-2004.

## Appendix A. Calculation of the diffusion coefficients in the azimuthal field

We consider a regular magnetic field with constant magnitude and azimuthal direction as in §5.2. We inject particles at  $\rho_0 = 8.5 \text{ kpc}$  or  $\rho_0 = 85 \text{ kpc}$  and we propagate them for 1 Mpc recording their trajectories. In this case we cannot use Eq. 16 to calculate the diffusion coefficients since the average values of the displacements we are considering are no longer 0 due to the drifts.

We proceed as follows: we build histograms of the particle positions at fixed times during the propagation and then we fit these histograms with gaussian distributions. The fitted value of the variance allows us to estimate the diffusion coefficient while the mean value of the distribution is related to the drift velocity.

The three directions we used to calculate the diffusion coefficients are:  $z$ ,  $\rho$  and  $\phi$ . The first two correspond to the two perpendicular coefficients and the latter to the parallel one. For  $z$  we simply histogram the  $z$  coordinate of the particles. For  $\rho$  we histogram the  $\rho = \sqrt{x^2 + y^2}$  and then we divide each bin in the histogram by  $\rho$  to take into account the volume element (in cylindrical coordinates). For  $\phi$  we histogram  $\phi \times \rho_0$ , where  $\rho_0$  is the distance at which the particles were injected.

In Fig. A1 we plot the three diffusion coefficients as a function of propagation time for injection at 8.5 kpc and  $\delta B/B = 0.5$ . The top panel represents the diffusion coefficient in the  $\rho$  direction, the middle panel the one in the  $z$  direction and the lower panel the parallel diffusion coefficient. The differently colored lines represent, from bottom to top, different energies from  $10^{15} \text{ eV}$  to  $10^{16.2} \text{ eV}$  with a logarithmic step of 0.2. The points to the far right of the plots are the average of the last 10 corresponding points and represent our estimate of the diffusion coefficient.

Concerning the parallel diffusion coefficient we can see that the curves are flat and that the diffusion regime is achieved. The only unexpected feature is in the two highest energy curves, corresponding to  $10^{16}$  and  $10^{16.2} \text{ eV}$  that show a steepening around  $c\tau \simeq 1 \text{ Mpc}$ . This steepening is simply due to the fact that at high energies and large propagation times some of the particles have enough time to complete half a circle around the “galaxy” and since to measure the parallel displacement we are using  $\phi \times \rho_0$ , particles with  $|\phi| > \pi$  end up in the wrong place in the histogram and distort the distribution. This is not however a physical effect and it is just a glitch of the method used to estimate the parallel displacement and we can just throw away the last few points and do the average with the remaining ones.

The diffusion coefficient along  $z$  shows a tiny sub-diffusion at low energies,  $D_z(E, \tau) \propto \tau^{-0.15}$ , that disappears by increasing the particle energy. It is interesting to note that in the plots of Fig. 1, that were obtained for similar parameters, but with the large scale field constant and along the  $z$  direction, the diffusion regime was obtained already with  $c\tau \sim 10 \text{ kpc}$ , with slightly larger times necessary for higher energies. In the present situation the results show that the opposite is occurring: at high energy the particles reach the diffusion regime, whereas at low energy they may not, at given time. In this case, since the instantaneous diffusion coefficient shows sub-diffusion, it is

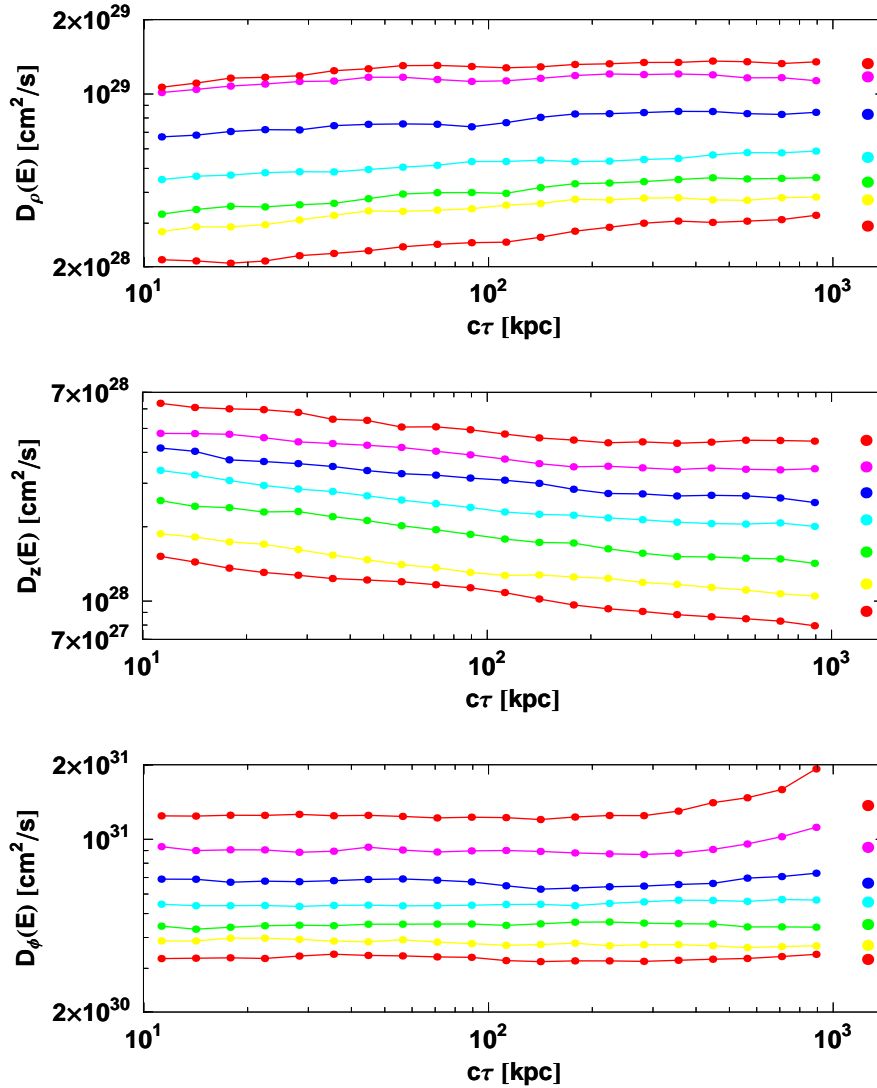


**Figure A1.** Instantaneous diffusion coefficients as a function of propagation time for injection at 8.5 kpc in a field composed of large scale azimuthal field and an isotropic turbulent field with  $\delta B/B_0 = 0.5$ . The three panels, from top to bottom, show the three diffusion coefficients along  $\rho$ ,  $z$  and  $\phi$  respectively.

not completely correct to define a diffusion coefficient using the average of the last few points. We do it anyway averaging the points with propagation times between 100 kpc and 1 Mpc that represent the range of propagation times obtained in Fig. 7 for energies between  $10^{15}$  eV and  $10^{17}$  eV. In this way we obtain at least a rough estimate of the diffusion coefficient affecting the particle propagation in our specific case.

For the diffusion coefficient in the  $\rho$  direction we have a situation similar to the  $z$  one, but with super-diffusion instead of sub-diffusion. In this case the effect is even smaller with:  $D_\rho(E, \tau) \propto \tau^{0.1}$ . Again increasing the energy the anomalous diffusion disappears.

Increasing the injection distance to 85 kpc the anomalous diffusion is reduced, but it is still slightly present. On the other hand increasing the turbulence level to  $\delta B/B_0 = 1$  or 2 reduces it much more than increasing the distance.

This is clear in the plots of Fig. A2 where we report the diffusion coefficients as a function of energy for the three levels of turbulence and the two injection distances. The black thick lines are the results for the case of constant large scale field directed along  $z$  (the curves of Fig. 3). The green lines are the diffusion coefficients in the  $\phi$  direction, the parallel ones. The red and blue lines are the diffusion coefficients in the  $\rho$  and  $z$  direction respectively. The solid lines are for injection at 8.5 kpc and the dotted ones for injection at 85 kpc.

The above caveat about anomalous diffusion notwithstanding, the plots in Fig. A2 seem to explain the results of Fig. 7. For the case of injection at 8.5 kpc and  $\delta B/B_0 = 0.5$  we found in §5.2 that the obtained escape time was bigger than the one we expected from the perpendicular diffusion coefficient. This is consistent with the results presented in Fig. A2 where it is shown that, in this case, the diffusion coefficient in the  $z$  direction is reduced and this obviously produces an increase in the escape time. Increasing the injection distance the  $z$  diffusion coefficient is closer to the “unmodified” one (see dotted blue line in the top panel of Fig. A2) and the times of escape are almost on top of the expectations (see light blue triangles and top black line in Fig. 7).

Increasing the level of turbulence, the effect of the curvature of the field lines is reduced and both the  $\rho$  and  $z$  diffusion coefficients rapidly converge towards the normal one (middle and bottom panels in Fig. A2).

## References

- [1] Blasi P and De Marco D, 2004 *Astropart. Phys.* **20** 559
- [2] Blasi P, 2005 *Mod. Phys. Lett. A* **20** 3055
- Hillas A M, 2005 *Journal of Physics G Nuclear Physics* **31** 95
- [3] Völk H J, Berezhko E G, Ksenofontov L T, 2005 *A&A* **433** 229 (and references therein)
- [4] Funk S, 2007 *Preprint astro-ph/0701471* (Review, accepted for publication in *Advances in Space Research (Proceedings COSPAR 2006)*)
- [5] Strong A W, Moskalenko I V and Ptuskin V S, 2007 *Preprint astro-ph/0701517* (To appear in the Annual Review of Nuclear and Particle Science, v.57)
- [6] <http://www.stanford.edu/imos/galprop.html>
- [7] Candia J, Mollerach S and Roulet E, 2003 *JCAP* **05** 003 (and references therein)
- [8] Harari D, Mollerach S and Roulet E, 2002 *JHEP* **07** 006 (and references therein)
- [9] Lee A A and Clay R W, 1995 *Journal of Physics G Nuclear Physics* **21** 1743
- [10] Zirakashvili V N *et al.*, 1998 *Astronomy Letters* **24** 139
- [11] Casse F, Lemoine M and Pelletier G, 2002 *Phys. Rev. D* **65** 023002
- [12] Giacalone J and Jokipii J R, 1999 *Ap.J.* **520** 204
- [13] Frigo M and Johnson S G, 2005 *Proceedings of the IEEE* **93** (2) 216  
<http://www.fft.w.org>
- [14] Parizot E, 2004 *Nucl. Phys. Proc. Suppl.* **136** 169
- [15] Jokipii R and Parker E, 1969 *Ap.J.* **155** 777
- [16] Beck, R, 2001 *Space. Sci. Rev.* **99** 243
- [17] Schlickeiser R, 2002 *Cosmic Ray Astrophysics* Springer (and references therein)

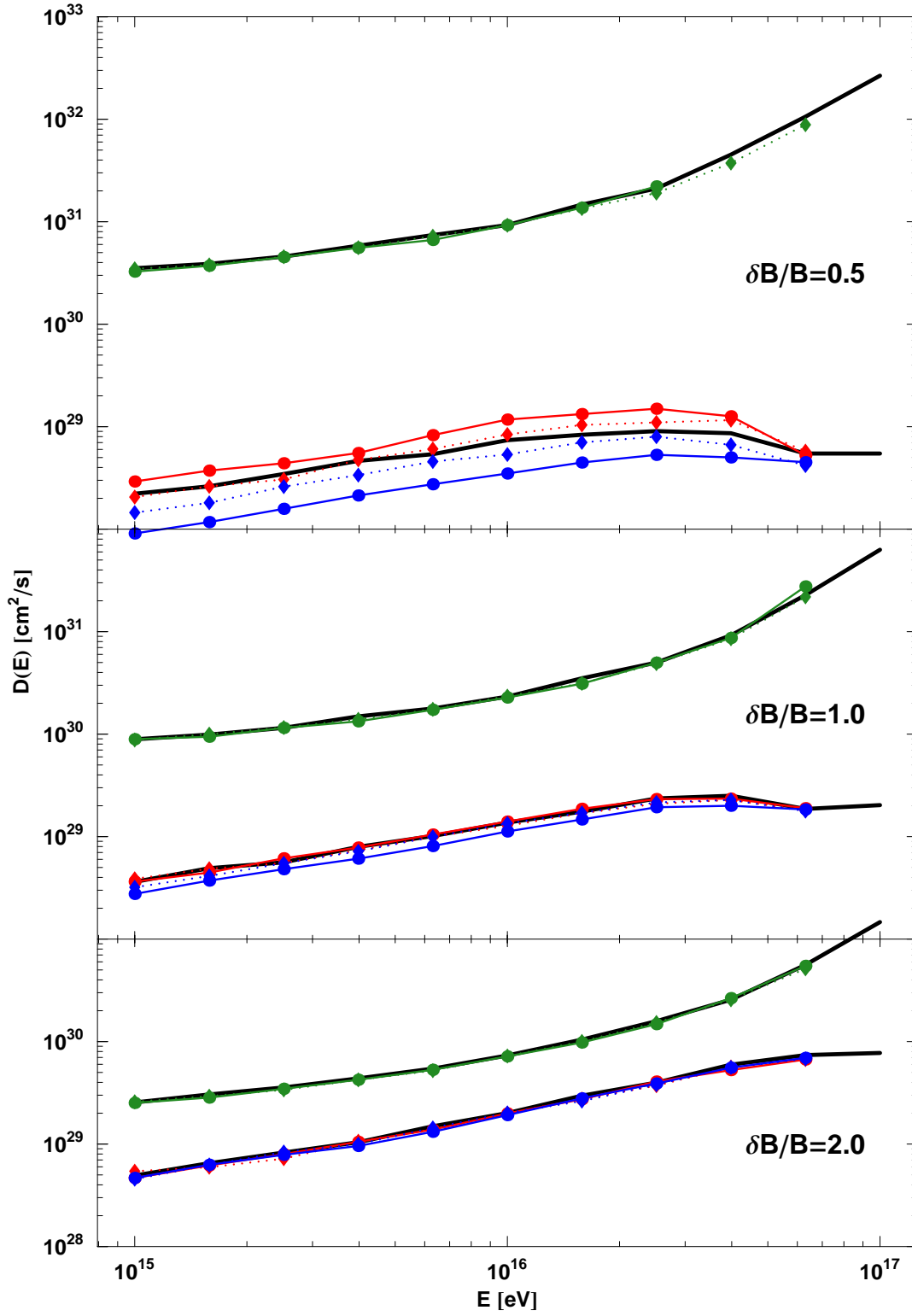


**Figure A2.** Diffusion coefficients as a function of energy. Green lines: parallel. Red lines: along  $\rho$ . Blue lines: along  $z$ . Black lines: parallel and perpendicular diffusion coefficients from Fig. 3. Solid lines: injection at 8.5 kpc. Dotted lines: injection at 85 kpc. The three levels of turbulence used are indicated in the panels.

- [18] Rossi B and Olbert S, 1970 *Introduction to the Physics of Space* McGraw-Hill.
- [19] Hoerandel J R, Kalmykov N N and Timokhin A V, 2007 *Astropart. Phys.* **27** 119
- [20] Phillipps S et al., 1981 *A&A* **103** 405
- [21] Zirakashvili V N, Breitschwerdt D, Ptuskin V S and Voelk H J, 1996 *A&A* **311** 113
- [22] Duvernois M A, Simpson J A and Thayer M R, 1996 *A&A* **316** 555